

FWI for model updates in large-contrast media

Sverre Brandsberg-Dahl¹, Nizar Chemingui¹, Alejandro Valenciano¹, Jaime Ramos-Martinez¹, and Lingyun Qiu¹

Abstract

We describe a new solution for recovering the long-wavelength features of a velocity model in gradient-based full-waveform inversion (FWI). The method uses reflected and transmitted wave modes to recover high-resolution velocity models. The new FWI gradient enables reliable velocity updates deeper than the maximum penetration depth of diving waves and reduces the FWI dependency on recording ultralong offsets. We also discuss a new FWI regularization scheme that overcomes the limitations of the inversion in the presence of high-contrast geobodies and cycle skipping. The solution utilizes a priori information about the earth model in the regularization as an extra term in the objective function. The implementation makes use of the split Bregman method, making it efficient and accurate. Results from applying the new FWI gradient to field data show that we can combine both transmitted and reflected energy in a global FWI scheme to obtain high-resolution velocity models without imprint of the reflectivity on the velocity updates. We illustrate the new regularization method's potential on the BP 2004 velocity benchmark model where our regularized FWI solution is capable of using a simple starting velocity model to deliver a high-quality reconstruction of salt bodies.

Introduction

Full-waveform inversion (FWI) is well established as a velocity estimation tool in the seismic industry. From the time FWI was introduced in the early 1980s by Tarantola, we had to wait almost 30 years until the technology achieved widespread acceptance. As stated, FWI has an intuitive and simple objective: minimize data misfit. However, in practice, this is clearly a complex task that requires the use of forward modeling to generate data, optimization algorithms, and regularization to help cope with the inherent nonlinearity of the problem.

The delay in uptake possibly can be attributed first to the (at the time) lack of cost-effective compute solutions powerful enough to solve the many forward modeling and imaging iterations needed as part of the FWI implementation. Seismic acquisition equipment and templates from this era also posed challenges: offsets were limited or even short, and recording systems were often equipped with harsh low-cut filters, effectively eliminating the low frequencies needed for FWI. It is important to keep in mind that the goal at the time was to acquire data for reflection seismology; little focus was put on the ability to record refractions and diving waves. Ocean-bottom-cable (OBC) and ocean-bottom-node (OBN) data were used in some early FWI applications as they circumvent these issues by decoupling the sources and receivers, providing long-offset, rich, and even full-azimuth coverage and more reliable recordings of low frequencies. Lately, applications to streamer data have become more widespread as the availability of long-offset data with good low-frequency content has increased. This has helped to truly establish FWI in the mainstream, in particular from a data-volume perspective as 3D streamer seismic

covers far more areas than nodes or OBC. Lately, use of multivessel acquisition schemes that can acquire very long offsets have further progressed this, enabling streamer-based recording of the diving waves and refractions that are so important for achieving convergence in most FWI schemes.

FWI inverts for the velocity model by solving a nonlinear inverse problem minimizing the difference between modeled data and recorded field data (Tarantola, 1984). The matching is quantified by the residuals of a least-squares objective function, and the model update is computed as a scaled representation of its gradient. For most, if not all, exploration seismic applications, FWI is an ill-posed problem due to the band-limited nature of the seismic data and the limitations of the acquisition geometries; we do not have access to the full wavefield. To mitigate this, typical FWI implementations involve iterative solution schemes with various forms of regularization applied to gradients and/or solutions. It is also common to approach FWI with a multiscale approach — i.e., starting from low frequencies and adding higher frequencies to the problem as the recovered model improves. Provided with the right data, FWI can produce high-resolution models of the subsurface when compared to ray-based methods.

Limitations to current implementations: Shallow water, reflectivity

Although well established as part of the velocity model building flow, most successful applications of FWI to date have been limited to shallow-water environments. This is because most implementations rely heavily on refracted energy or diving waves. Put this together with the offset limitations that exist in seismic data — stream and node alike — and it follows naturally that shallow settings lend themselves easiest to being addressed by FWI as they are better sampled by refractions. Liu et al. (2012) gave a recent application of FWI to shallow-water OBC in which accurate overburden velocities were obtained using refractions. This not only improved the shallow imaging but also resolved depth ambiguities and mis-ties at reservoir level. A similar case using data from a dual-sensor towed-streamer acquisition was presented by Zou et al. (2014) in which the authors show that modern streamer data contains refractions that produce good FWI velocity updates to a depth of about one-fourth of the streamer length. In these scenarios, FWI relied mainly on recorded diving waves to resolve small-scale geologic features up to the deepest turning point. For deeper targets, FWI needs to rely on reflected energy to update the model. However, as we will discuss later in this article, using the conventional FWI gradient computation in such situations is challenging unless the recorded reflections have extraordinary low-frequency content.

Beyond the depth limitations of refractions, a range of factors will influence how well FWI will resolve the velocities in the subsurface. A key role is played by the rock formations over which the seismic was acquired; harder rocks (well consolidated) tend

¹PGS.

<http://dx.doi.org/10.1190/tle36010081.1>

to have good correlation between velocity and reflectivity, which is a common assumption in most FWI implementations. A typical FWI scheme uses an explicit relationship between density and velocity in the forward-modeling step, such as Gardner's relation, so there is an intrinsic assumption that change in reflectivity is also a change in velocity. However, in many softer rocks and unconsolidated sediments, the reflectivity is typically correlated to density changes and not velocity changes, as the latter is typically driven by pressure changes, burial history, etc. When applying FWI in basins with such characteristics, for example in the Gulf of Mexico, great care must be taken to avoid that the FWI updates not only maps reflectivity into the velocity model. FWI might produce a "pretty" velocity field, but it is often an erroneous representation of what is actually happening in the subsurface.

To move beyond the typical limitations outlined above, there has been a flurry of activity in recent years to reformulate FWI algorithms to include reflected energy for retrieving long-wavelength updates (e.g., Xu et al., 2013; Zhou et al., 2015, Alkhalifah, 2015). The fundamental idea is to compute a gradient in which undesired reflectivity is not present, such that the full wavefield can be used in FWI to produce high-resolution velocity models that correctly predict refractions and reflections — a key step when using the models for depth migration and imaging. These improvements to the physics of FWI are nicely complemented by the introduction of new regularization schemes to stabilize the solution to the inversion step of FWI — i.e., improving the implementation's mathematics. FWI is particularly challenged when facing large-contrast geobodies such as salt bodies or volcanics. In such situations, the FWI solution often gets trapped in local minima unless the starting model is very accurate. Introduction of total variation (TV) regularization (Guo and de Hoop, 2013) and, most recently, the use of vertical hinge-loss asymmetric TV (Esser et al., 2015), have offered important insights into how such situations can be mitigated when applying FWI to large-scale field data sets.

In the following pages, we will propose and review the concepts behind a new FWI gradient implementation that eliminates the migration isochrones that typically dominate FWI gradients in heterogeneous media. By separating low-wavenumber from high-wavenumber components in the gradient, we can produce long-wavelength velocity updates at depths greater than the penetration depth of the diving waves. This is followed by a discussion of how we have generalized the ideas of Esser et al. (2015) by combining the variable weighted L^1 norm of the total variation of the model with a weighted version of the model spatial variability. The variable regularization parameters allow refinement of the sediments region of the model with a mild regularization, while promoting sharp contrast and constant velocity geobodies in a different region with a strong regularization. Several data examples, both synthetic and

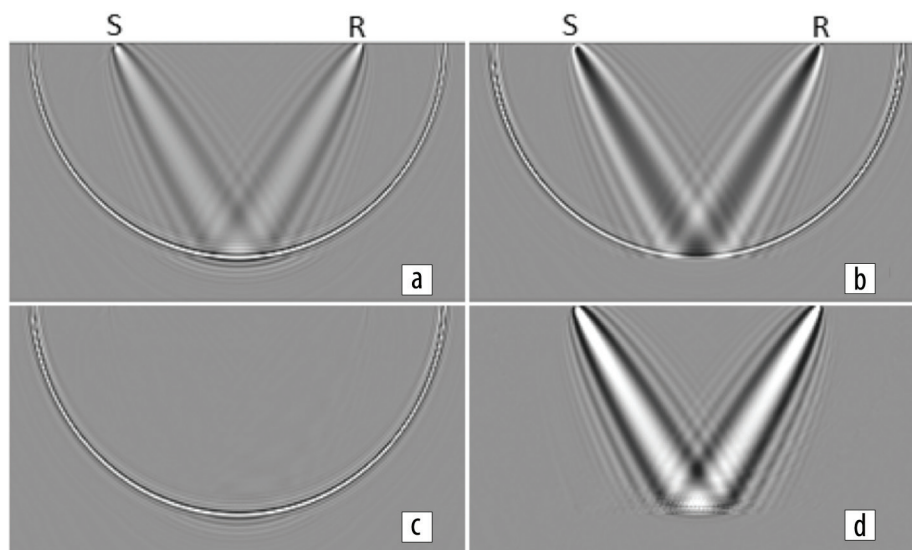


Figure 1. Sensitivity kernels of a source-receiver pair in a model with a homogeneous layer overlying a halfspace: (a) bulk modulus, (b) density, (c) impedance, and (d) velocity.

field data, highlight the method's performance aspects. Our new solutions are able to provide high-resolution velocity models from records containing diving waves and reflections without the migration imprint provided by conventional FWI.

A robust gradient for macro-velocity model updates

In conventional FWI, we solve a nonlinear inverse problem by iteratively updating the model to minimize an objective function, which is the difference between the modeled seismic data and the recorded field data. This misfit function is generally minimized in a least-squares sense, and the model update is computed as a scaled representation of its gradient. In the case of an isotropic acoustic medium parameterized in terms of bulk-modulus and density (κ, ρ), Tarantola (1984) shows that the gradient depends on the kernels for κ and ρ that can be written as:

$$K_{\kappa}(\mathbf{x}) = \frac{1}{\kappa(\mathbf{x})} \int \frac{\partial S(\mathbf{x}, t)}{\partial t} \frac{\partial R(\mathbf{x}, T-t)}{\partial t} dt \quad (1)$$

and

$$K_{\rho}(\mathbf{x}) = \frac{1}{\rho(\mathbf{x})} \int \nabla S(\mathbf{x}, t) \cdot \nabla R(\mathbf{x}, T-t) dt, \quad (2)$$

where $\kappa(\mathbf{x}) = \rho(\mathbf{x})v^2(\mathbf{x})$ is the equation that relates the bulk modulus to velocity, $S(\mathbf{x}, t)$ is the source wavefield, and $R(\mathbf{x}, T-t)$ is the residual wavefield after time reversal. Equations 1 and 2 are sensitivity kernels for the respective parameter and measure the variation in the misfit function caused by change in that parameter while holding the others fixed. The sensitivity kernels corresponding to equations 1 and 2 for a simple two-layer model are shown in Figures 1a and 1b. Note how the back-scattered energy in the kernels, or "rabbit ears," changes polarity in the two images. This fact was recognized in the work of Whitmore and Crawley (2012)

who introduced a new reverse time migration (RTM) imaging condition formed by the summation of two kernel components to suppress low-wavenumber imaging artifacts. For the RTM application, the aim was to remove the low wavenumbers — quite opposite of what we aim to do for FWI. Using the sensitivity kernels in equations 1 and 2, we can express new kernels in terms of bulk modulus and density by simply forming linear combinations

$$K_v(\mathbf{x}) = K_K(\mathbf{x}) - K_\rho(\mathbf{x}) \quad (3)$$

$$K_z(\mathbf{x}) = K_K(\mathbf{x}) + K_\rho(\mathbf{x}), \quad (4)$$

where the impedance kernel in equation 4 can be recognized as the RTM imaging condition presented by Whitmore and Crawley (2012). The impedance kernel comprises the high-wavenumber components of the velocity field while removing the unwanted backscattered noise. The examples presented in their paper, using heterogeneous models, highlighted the importance of dynamically weighting the different components of the impedance kernel to achieve optimal removal of the low-wavenumber artifacts. Figure 1c shows the result of weighting the components from Figures 1a and 1b to produce an RTM impulse response free of back-scattered noise.

On the other hand, the velocity kernel given by equation 3 is ideal for FWI where the low-wavenumber components of the gradient are preferred. As we know, the high wavenumbers associated with reflections may mislead the inversion. Following the premises of Whitmore and Crawley (2012), an FWI gradient can be derived by dynamically weighting the velocity sensitivity kernel (equation 3). Their dynamic weights can be adapted to alternatively remove the high wavenumbers from the FWI gradient in a heterogeneous media. The new FWI gradient derived from equation 3 is:

$$G(\mathbf{x}) = \frac{1}{2A(\mathbf{x})} \left\{ \int_t \left[W_1(\mathbf{x}, t) \frac{1}{v^2(\mathbf{x})} \frac{\partial S(\mathbf{x}, t)}{\partial t} \frac{\partial R(\mathbf{x}, T-t)}{\partial t} \right] dt - \int_t \left[W_2(\mathbf{x}, t) \nabla S(\mathbf{x}, t) \cdot \nabla R(\mathbf{x}, T-t) \right] dt \right\} \quad (5)$$

where $W_1(\mathbf{x}, t)$ and $W_2(\mathbf{x}, t)$ are dynamic weights designed to optimally suppress the migration isochrones, and $A(\mathbf{x})$ is the illumination term. Figure 1d is produced using equation 5; it illustrates how the migration isochrone has been removed while the low-wavenumber energy is preserved.

Figure 2a shows the conventional FWI gradient compared to the modified gradient from equation 5 (Figure 2b) in a simple $v(z)$ velocity model where velocity is linearly increasing with depth. Here, the modified gradient in equation 5 removes the migration operator (isochrone) but preserves all the low-wavenumber components associated with the diving waves (“bananas”) and backscattering (“rabbit ears”). To better illustrate the use of reflections in FWI, we use a simple 2D synthetic example consisting of five homogeneous layers, as shown in Figure 3. The data has maximum offsets of 4 km, so only precritical reflections are

used in the inversion. The starting velocity model for FWI contained errors up to 100 m/s. The inversion was performed on a frequency band of 3–5 Hz. Figures 3b and 3c show the results of the inversion using the conventional FWI gradient as compared to our new FWI gradient. Results from the new gradient are accurate and do not suffer from the high-wavenumber artifacts observed on the conventional FWI update, which is dominated by the reflections as would be observed in a migrated image.

Stabilizing FWI solutions with regularization

With the improved FWI gradient introduced in the previous section, we move on to the practicalities of how to regularize the FWI problem and solutions. As mentioned in the introduction, our approach to overcome such challenges uses a combination of total variation (TV) regularization (Guo and de Hoop, 2013) and the vertical hinge-loss asymmetric TV (Esser et al., 2015). This allows us to recover relatively complex velocity models, even when starting from a simple starting model.

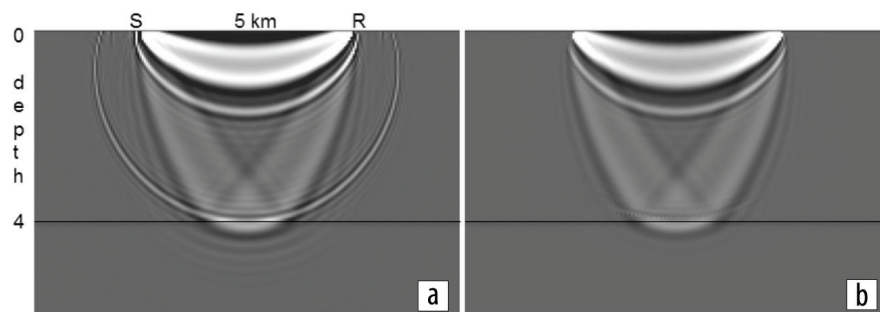


Figure 2. Sensitivity kernels of a source-receiver pair in a model with a $v(z)$ layer overlying a half-space: (a) conventional kernel and (b) dynamically weighted velocity kernel.

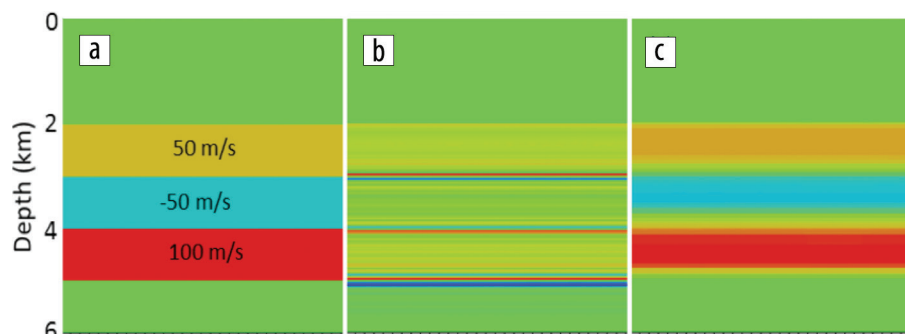


Figure 3. Five-layer synthetic model: (a) Difference between exact and starting model, and between the inverted and the initial velocity model using the (b) conventional and (c) new FWI gradients.

The main advantage of the L^1 -TV regularization is that the sharp edges are well preserved while the artifacts and noise are efficiently removed during inversion. In other words, the L^1 -TV regularization pursues a sparse representation of the model in the space spanned by piecewise constant functions. Full-waveform inversion with L^1 norm TV regularization can be formulated as the optimization problem

$$\min_m \|F(m) - u\|_2^2 + \lambda \|\nabla m\|_1, \quad (6)$$

where F is the modeling operator, m is the velocity model, u is the recorded data, and λ is the regularization parameter. The second term in equation 6 uses the L^1 norm to pursue a sparse representation of the high-contrast boundaries of the model. The L^1 norm can be calculated by using different approximations (e.g., Guitton and Symes, 2003). However, slow convergence has been observed when using those approximations to achieve a sparse solution. Our L^1 norm implementation solves the slow convergence problem by using the split Bregman iterations. This method has proved efficient for solving L^1 optimization problems, in particular for TV regularization as shown by Goldstein and Osher (2009). In their work, they showed that the optimization problem as expressed in equation 6 can be reformulated as

$$\min_{m,d} \|F(m) - u\|_2^2 + \lambda \|d\|_1 + \frac{\gamma}{2} \|d - \nabla m - b\|_2^2, \quad (7)$$

where $d = \nabla m$ is used as an expansion of the model space, and the auxiliary variable b is updated according to $b_{k+1} = b_k + \nabla m - d_{k+1}$. In the next section, we adapt this split Bregman algorithm to accommodate the objective function with the steerable variation term.

The L^1 -TV norm regularization with constant regularization parameter (λ) treats all regions in the model with homogeneous isotropic weights. Ideally, by including additional constraints, we would like to add any prior physical information about the model to steer the solution in any direction. We call this novel method “steerable variation regularization.” Full-waveform inversion with steerable variation regularization can be formulated as the following optimization problem:

$$\min_m \|F(m) - u\|_2^2 + \|\lambda \nabla m\|_1 + \int_{\Omega} \nabla m \cdot P, \quad (8)$$

where the steering field P is used to introduce any a priori knowledge of the velocity model. The dot product of the gradient of the model and the direction indicated by P can be considered the changing rate of the model along the steering field. Without taking the absolute value, we not only can control the magnitude of ∇m (with the TV) but also guide its direction with the second regularization term. The steering field P plays a crucial role in our inversion algorithm and is updated during the FWI iterations. As initial value, we typically use pre-existing models such as a legacy velocity model or a starting model generated from

conventional VMB. If limited a priori information is available, we are also able to use any preliminary seismic images, such as a sediment flood, for the purpose of an initial model. As this is available at early stages of the velocity model building workflow, it can be incorporated easily into our regularization strategy in the absence of a legacy model.

To design the FWI workflow with steerable regularization, we follow a slightly modified multiscale approach, where the principle is to reconstruct the model’s high-contrast components in the first stages and then add the details in later iterations. To ensure convergence of FWI, we typically run many stages where we relaxed the regularization as necessary to define the high-contrast events while preserving the high resolution in the sediments. Thus, it is preferable to choose a spatially variant regularization parameter λ for the TV regularization. It provides the flexibility to target the area in which, based on the a priori information, salt bodies may exist without tremendously increasing the inversion’s computational cost. With a spatially variant regularization parameter, we can build the salt and refine the sediments at the same time without precise knowledge of the salt boundaries position. In that case, the salt does not necessarily need to be included in the initial model and rather can be used as a soft constraint in the regularization. The main reason behind this is that the synthetic data is sensitive with respect to the model, but the optimal regularization parameter is not. Hence, if we have inaccurate information on the salt boundaries, it might be preferable to include that prior information in the regularization parameter rather than in the misfit term.

Examples

To illustrate the ability of our new FWI scheme to deal with large contrast media, we use a modified version of the BP 2004 benchmark velocity model (shown in Figure 4a) (Billette and Brandsberg-Dahl, 2005). The model contains two salt bodies with unique characteristics (different velocity, size, and geometry). These properties promote better illumination, by the refracted/diving waves, of the “tooth” salt body to the right of the model than for the salt body to the left. The synthetic data was created with a minimum frequency of 3 Hz and a maximum offset of 12 km.

The starting velocity model for the FWI consists of an average $v(z)$ gradient hung from the water bottom (Figure 4b). Note that the initial model does not contain any high-contrast velocity information, but, at the same time, it is not too far away from the true sediments velocities. Several stages were used to improve the convergence of the FWI and avoid local minima by starting at low frequencies and working up to higher frequencies. As our algorithm is implemented in the time domain, we use band-passed versions of the data as input, with consecutively increasing center frequencies of 5 Hz, 9 Hz, 12 Hz, 15 Hz, and 18 Hz. For a fair comparison, the same number of frequency bands and number of iterations were used for all the compared algorithms. For the FWI with TV regularization, a constant regularization parameter was applied with the same decay rate as in the steerable variation regularization scheme.

Figures 4c, 4d, and 4e show the inversion results with and without regularization. Figure 4c displays the result of FWI without regularization, Figure 4d shows the result of the FWI with TV

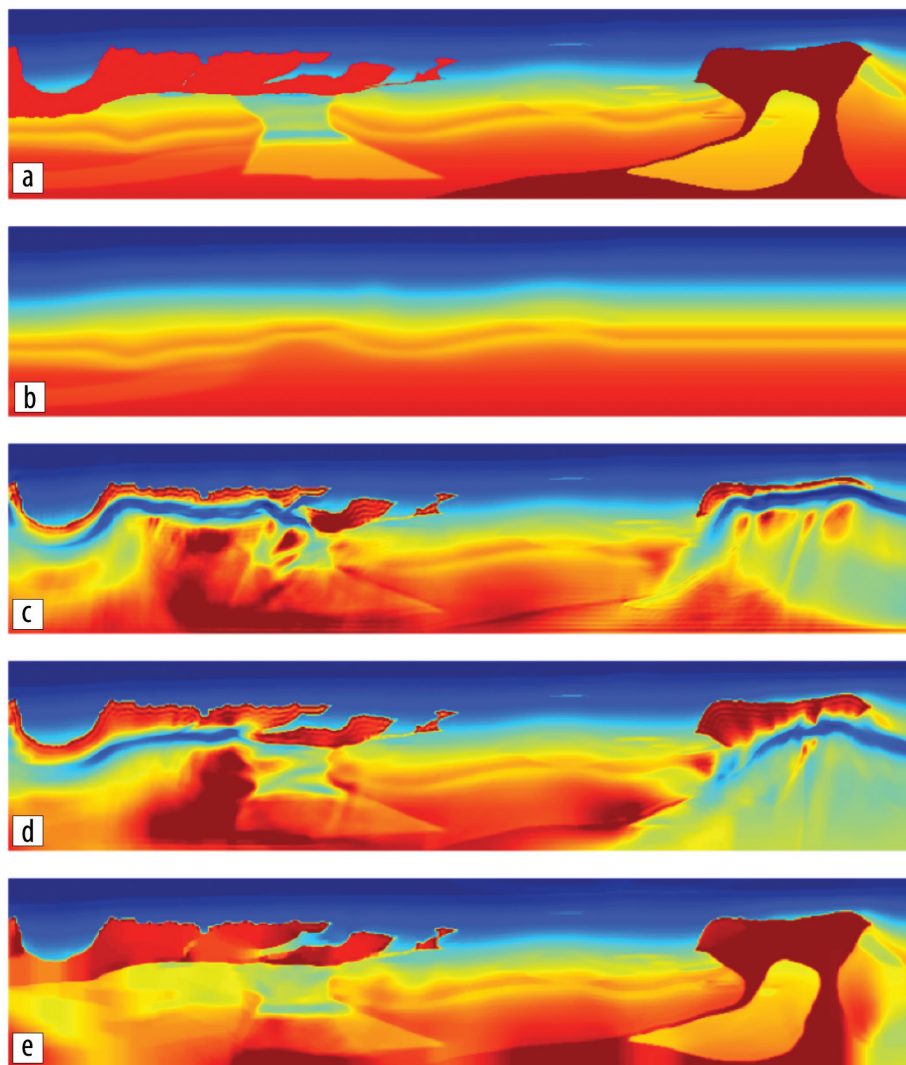


Figure 4. Comparison of different regularization methods: (a) true model, (b) starting model, (c) FWI without regularization, (d) FWI with TV regularization, and (e) FWI with steerable variation regularization.

regularization and constant regularization parameter, and Figure 4e shows our result when steerable regularization was used. Note how significant artifacts due to cycle skipping are observed in the result using conventional FWI. With TV regularization and a proper choice of the regularization parameter, the artifacts can be reduced and the result is improved, but the cycle skipping is still visible. Our FWI with steerable regularization obtains the best result by defining the top and bottom salt boundaries and the correct velocity of the sediments below salt. In the right side of the model, the conclusions from comparing the different regularizations are the same as the left side of the model, even though the starting velocity is farther away from the true model.

To further illustrate the impact of the new FWI gradient, we use field data from deepwater Gulf of Mexico (DeSoto Canyon). The data were acquired with dual-sensor streamers and with a maximum offset of 12 km. The FWI full-power frequency band was 3–7 Hz. No particular mutes or event selections were used, therefore all recorded data were employed during the inversion. Figure 5a shows an overlay of the initial velocity model on the seismic image. Figures 5b and 5c show the updates from the

conventional and the new gradients, respectively. The update from the conventional FWI is basically a mapping of the reflectivity or image into the velocity model, as is clear when compared to Figure 5a. When contrasted to the update from FWI with the new gradient, we can observe longer wavelength updates to the model to follow geology but that do not constitute a simple mapping of reflectivity into the velocity field. To further evaluate the model derived from the new gradient, we performed Kirchhoff depth migration. We observed that the new FWI velocity model improved the flatness of the offset gathers as shown in Figures 5a and 5b.

As our final example, we show results for a wide-azimuth dual-sensor data set acquired in deepwater Gulf of Mexico with maximum inline and crossline offsets of 7 km and 4.2 km, respectively. Here we deployed the new gradient combined with TV regularization. No steering field was deployed in this case. Figures 6a and 6b show depth slices (1440 m and 1620 m) of the initial velocity model computed from reflection tomography. We perform FWI from this model using a frequency bandwidth of 3–5 Hz. For wavefield extrapolation, we use the pseudoanalytical method assuming a TTI medium with variable density. Figures 6c and 6d show the corresponding slices for the inverted model. As observed, the new gradient allows updates to resolve small-scale

lateral heterogeneities in the velocity model, provided mainly by the presence of diving waves. At the same time, there is no migration imprint in the updates produced by the specular reflections as observed in the vertical profiles for the starting and the inverted velocity models (Figures 7a and 7b).

Summary

We have described a new robust solution for recovering the long-wavelength features of a velocity model in gradient-based FWI. The method uses reflected and transmitted wave modes to recover high-resolution velocity models. The new FWI gradient enables reliable velocity updates deeper than the maximum penetration depth of diving waves and reduces the FWI dependency on recording ultralong offsets. Results from applying the new FWI gradient to field data show that we can combine both transmitted and reflected energy in a global FWI scheme to obtain high-resolution velocity models without imprint of the reflectivity on the velocity updates.

We also have presented a new FWI regularization scheme that can overcome the limitations of the inversion in the presence of

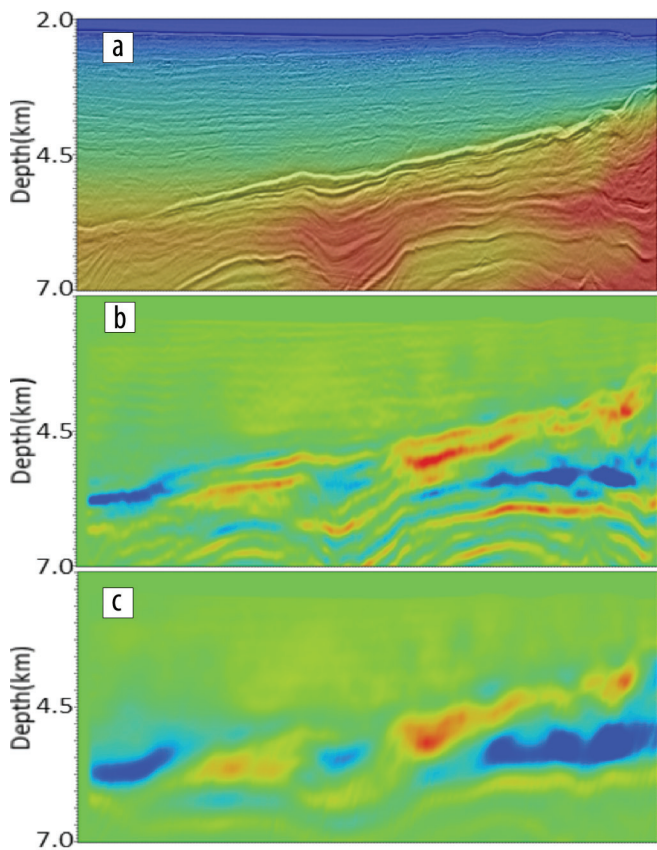


Figure 5. 2D dual-sensor data example from deepwater Gulf of Mexico: (a) initial velocity model overlaid by the seismic image, (b) conventional FWI model update, and (c) new FWI model update.

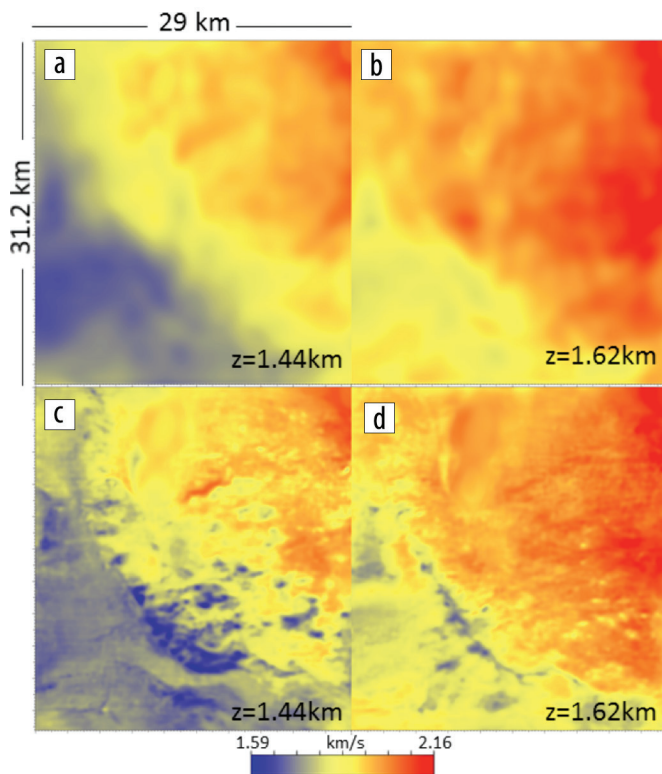


Figure 6. Results for the wide-azimuth Gulf of Mexico dual-sensor data example new FWI gradient and TV regularization.

high-contrast geobodies and cycle skipping. It allows the use of a priori information about the earth model in the regularization as an extra term in the objective function. The implementation makes use of the split Bregman method, making it efficient and accurate. The numerical experiments demonstrate that our algorithm can deal with the challenges of the presence of high-contrast geobodies and cycle skipping. We show how the steering regularization terms can drive the solution out of local minima. However, it remains to be demonstrated that this kind of constraint on the solution can help the inversion deal with the same problems with field data. The errors in the physics used for the modeling operator and the noise in the data could demand the use of a better approximation of the wave propagation in the subsurface as well as better data-selection techniques. **11**

Corresponding author: Nizar.Chemingui@pgs.com

References

- Alkhalifah, T., 2015, Conditioning the full-waveform inversion gradient to welcome anisotropy: *Geophysics*, **80**, no. 3, R111–R122, <http://dx.doi.org/10.1190/geo2014-0390.1>.
- Billette, F. and S. Brandsberg-Dahl, 2005, The 2004 BP velocity benchmark: 67th Conference & Exhibition, EAGE, Extended Abstracts.
- Esser, E., L. Guasch, T. van Leeuwen, A. Y. Aravkin, and F. J. Herrmann, 2015, Total variation regularization strategies in full waveform inversion for improving robustness to noise, limited data and poor initializations: Technical Report, TR-EOAS-2015-5.
- Goldstein, T., and S. Osher, 2009, The split Bregman method for L1-regularized problems: *SIAM Journal on Imaging Sciences*, **2**, no. 2, 323–343, <http://dx.doi.org/10.1137/080725891>.
- Guitton, A. and Symes, W., 2003, Robust inversion of seismic data using the Huber norm: *Geophysics*, **68**, no. 4, 1310–1319, <http://dx.doi.org/10.1190/1.1598124>.
- Guo, Z., and M. V. de Hoop, 2013, Shape optimization and level set method in full waveform inversion with 3D body reconstruction:

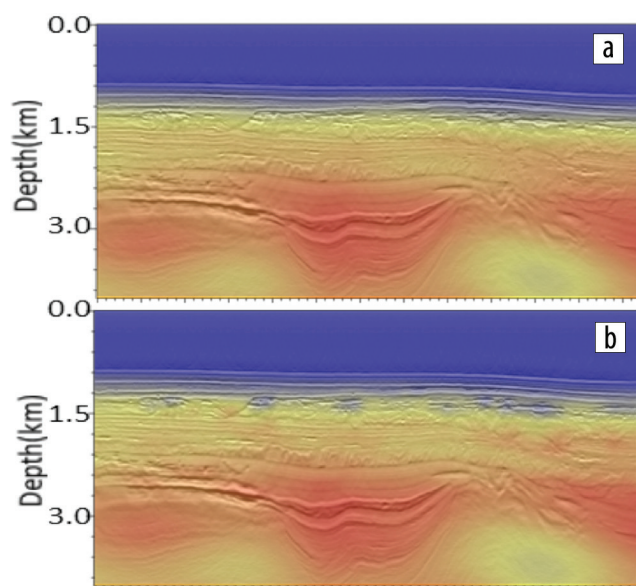


Figure 7. Results for the wide-azimuth Gulf of Mexico dual-sensor data example using the dynamically weighted gradient. Vertical profiles for the (a) starting and the (b) inverted velocity model overlaid by the corresponding migrated stacked images. Horizontal distance is 18.6 km.

- 83rd Annual International Meeting, SEG, Expanded Abstracts, 1079–1083, <http://dx.doi.org/10.1190/segam2013-1057.1>.
- Liu, F., L. Guash, S. C. Morton, M. Warner, A. Umpleby, Z. Men, S. Fairhead, and S. Chekles, 2012, 3D time-domain full waveform inversion of a Valhall OBC dataset: 82nd Annual International Meeting, SEG, Expanded Abstracts, <http://dx.doi.org/10.1190/segam2012-1105.1>.
- Tarantola, A., 1984, Inversion of seismic reflection data in the acoustic approximation: *Geophysics*, **49**, no. 8, 1259–1266, <http://dx.doi.org/10.1190/1.1441754>.
- Whitmore, N. D., and S. Crawley, S., 2012, Application of RTM inverse scattering imaging conditions: 82nd Annual International Meeting, SEG, Expanded Abstracts, <http://dx.doi.org/10.1190/segam2012-0779.1>.
- Xu, S., D. Wang, F. Chen, Y. Zhang, and G. Lambare, 2013, Full waveform inversion for reflected seismic data: 74th Conference & Exhibition, EAGE, Extended Abstracts, <http://dx.doi.org/10.3997/2214-4609.20148725>.
- Zhou, W., R. Brossier, S. Operto, and J. Vireux, 2015, Full waveform inversion of diving waves for velocity model building with impedance inversion based on scale separation: *Geophysical Journal International*, **202**, no. 3, 1535–1554, <http://dx.doi.org/10.1093/gji/ggv228>.
- Zou, K., J. Ramos-Martínez, S. Kelly, A. A. Valenciano, N. Chemingui, and J. Lie, 2014, Refraction full-waveform inversion in a shallow water environment: 76th Conference & Exhibition, EAGE, Extended Abstracts, <http://dx.doi.org/10.3997/2214-4609.20141415>.